1.2 ANALYSES OF SPACEBORNE DOPPLER RADAR SYSTEM PERFORMANCE ON MEASURING VERTICAL RAINFALL VELOCITY

Simone Tanelli[1*], Eastwood Im [1], Stephen L. Durden [1], and Luca Facheris [2]
[1] Jet Propulsion Laboratory, California Institute of Technology, Pasadena CA, USA
[2] Dipartimento di Ingegneria Elettronica - Università di Firenze - Firenze - Italy

1. INTRODUCTION

The importance of the motion of air masses at all scales of atmospheric circulation has brought substantial development of the Doppler radar technology in the field of precipitation monitoring. Although techniques have been developed in the last two decades for ground-based and airborne Doppler weather radars (Doviak and Zrnic, 1993 and Hildebrand and Moore 1990), they do not fully address the issues pertained to spaceborne radars. These unique issues arise from the downward viewing geometry with a fast moving (*i.e.,* $v_S \cong 7$ km/s for Low Earth Orbiting (LEO) satellites) orbiting platform and a relatively large volume of resolution (*e.g.*, 2km footprint radius and 250m range resolution).

The spaceborne precipitation radar studied in this paper is cross-track scanning and with a small scan angle β (*e.g.*, $\beta < 5$ deg.). It will be referred to as Nadir-looking Doppler Precipitation Radar (NDPR). This viewing geometry allows to measure the average vertical motion v_R of the hydrometeors by calculating the first moment of the measured Doppler velocity spectrum. Such measurements, in turn, allow to estimate the vertical wind and, in particular, its gradient in the vertical direction which is a fundamental quantity to derive the vertical fluxes of latent heat.

Measurements of mean Doppler velocity at off-nadir angles are affected by contributions from horizontal winds. As thoroughly discussed in Amayenc et al. (1993), these contributions could be identified and removed only through a Doppler radar system with multiple-angle viewing geometry or by adopting some assumptions on the continuity of the velocity field. However, under the assumption of small β, these contributions are in general small and can be neglected.

Measurements of the rainfall average vertical velocity v_R are affected by several errors. These errors are briefly described here, and discussed in depth in the remainder of this paper.

- *Errors of the spectral moment estimator (SME)*: The estimate x_m of the m-th spectral moment calculated from the returns of M radar pulses is a random variable typically described through its expected value $\langle x_m \rangle$ and standard deviation $\sigma(x_m)$. These two statistics depend on the characteristics of the random process associated with the rainfall radar signal and on the performance of the specific SME algorithm adopted to calculate x_m. In particular, when the signal has a Gaussian Doppler spectrum, the statistics of x can be calculated from the following parameters: a) the normalized width $w_N = w\ 2\ /\ (\lambda\ PRF)$, where w is the Doppler velocity spectral width of the signal, *PRF* is the radar Pulse Repetition Frequency and λ is the radar operating wavelength, b) the Signal to Noise Ratio (*SNR*), c) the normalized mean Doppler velocity $v_N = v\ 2\ /\ (\lambda\ PRF)$ and, d) the number of samples (M). Performances of the most widely used SME algorithms for a wide range of these parameters are discussed in Section 2. In Section 3, it is shown that, when observing a homogeneous rain field, the Doppler velocity spectrum can be approximated by a Gaussian. Also, the criteria to calculate the spectral parameters from the NDPR configuration parameters are here described.
- *NUBF-induced bias:* when the radar is observing a non-homogeneous rainfall field, the contributions to the Doppler spectrum from different portions of the resolution volume are unevenly weighted. Since each spectral contribution is subject to a Doppler shift proportional to the along-track

* *Corresponding author address:* Simone Tanelli, Jet Propulsion Laboratory, 4800 Oak Grove Dr. MS 300-243, Pasadena CA 91109; e-mail: simone.tanelli@jpl.nasa.gov

displacement of the corresponding portion with respect to the cross-track plane, the inhomogeneous weighting modifies the spectral shape and induces a bias in the estimates of vertical velocity. The NUBF-induced bias is discussed in Section 4.

- *Pointing-induced bias:* when the radar viewing angle is offset with respect to the cross-track plane, a bias in vertical velocity estimates proportional to the offset angle α is observed.
- *Errors induced by the surface-clutter:* the surface backscattered power can contaminate the radar return even for volumes of resolution that do not (nominally) intersect the surface. Such clutter is received through the antenna sidelobes and/or through the range weighting function (because of the finite receiver bandwidth). The spectrum of the clutter signal can assume different shapes depending on the geometry of the problem. The impact of the surface clutter is discussed in Section 5.

2. PERFORMANCES OF SPECTRAL MOMENTS ESTIMATORS

The two most widely used categories of algorithms for Spectral Moments Estimators (SME) of weather radar signals are the Pulse Pair (PP) processing and the spectral analysis through Discrete Fourier Transform (DFT). In recent studies their performances have been analyzed focusing on their application to spectra measured by NDPR (Tanelli et al. 2002). The results of these studies are summarized here for 4 DFT-based SME algorithms. The mean velocity estimate is calculated as:

$$\hat{v} = -\frac{\lambda}{2MT_S} m_0 = \\ = -\frac{\lambda}{2MT_S} \left\{ \begin{array}{l} m_0' + \dfrac{1}{(S_S + S_N) - \hat{S}_N} \cdot \\ \cdot \displaystyle\sum_{m=m_0'-M/2}^{m_0'+M/2} (m - m_0') \cdot \left[\tilde{P}_{\mathrm{mod}_M(m)} - \hat{N}_{\mathrm{mod}_M(m)} \right] \end{array} \right\} \quad (1)$$

where S_S and S_N are the signal and noise power, respectively, $\hat{S}_N$ is the estimated mean noise power, P_m is m-th line of the power spectrum as calculated through DFT of M complex voltage samples (*periodogram*), $\hat{N}_m = \hat{S}_N / M$ is the estimated noise spectral density, and m_0' is the number of a specific frequency bin in which the initial estimate α of the mean spectral frequency is made (i.e., $m_0' = \alpha\, M / PRF$).

The four algorithms are different in their ways of handling of noise and strategy for obtaining the initial guess α. The first algorithm, referred to as DFT-Z, assumes $m_0' = 0$. It does not remove any white noise contribution (*i.e.*, $\hat{S}_N = 0$ in (1)), which makes it a biased estimator at low SNR's. The second algorithm, referred to as DFT-ZN, also assumes $m_0' = 0$ but it removes the nominal power (i.e., $\hat{S}_N = S_N$) in order to eliminate the bias due to white noise. However, as shown by Sirmans and Bumgarner (1975), at low SNR's the standard deviation of (1) for DFT-ZN is significantly higher than that for DFT-Z.

The third algorithm, referred to as DFT-M, was suggested by Zrnic (1979). It assumes m_0' to be equal to the number of the frequency bin which has the largest power (*i.e.*, $m_0' : \tilde{P}_{m_0'} = \max\{\tilde{P}_k\}$), and it does not remove any white noise contribution. For narrow spectra (*e.g.*,w_N < 0.1) and large M (e.g., M>1000), this algorithm provides unbiased estimates of the first spectral moment with the corresponding standard deviations comparable to those obtained by DFT-Z. However, this algorithm is more sensitive to w_N than DFT-Z and DFT-ZN (Tanelli et al. 2002b).

The fourth algorithm, referred to as 'two-step' DFT algorithm (DFT-2), was recently introduced by Tanelli et al. (2002) to provide better performances for spaceborne applications. In the first step of this algorithm, (1) is applied with $m_0' = 0$ and $\hat{S}_N = S_N$ to obtain a first velocity estimate $\hat{v}^{(1)}$. $\hat{S}_N$ is then updated by setting it equal to the minimum of the smoothed periodogram. In the second step, a refined velocity estimate $\hat{v}^{(2)}$ is obtained through (1) with $m_0' = \hat{v}^{(1)} / (-\lambda / 2MT_S)$ and with the updated $\hat{S}_N$. This second step can be repeated until $\left| \hat{v}^{(i)} - \hat{v}^{(i-1)} \right|$ falls below a specified threshold. In general, this algorithm is capable of providing unbiased estimates with standard deviations comparable to DFT-Z. For mean vertical velocities v_c close to the Nyquist limit $v_m = PRF\lambda/4$, it shows a multimodal distribution of the mean velocity estimate, with the secondary modes appearing at $v_c \pm 2v_m$ and $v_c \pm v_m$. However, these secondary modes are easily removed by checking if a) $|\hat{v}| > v_m$

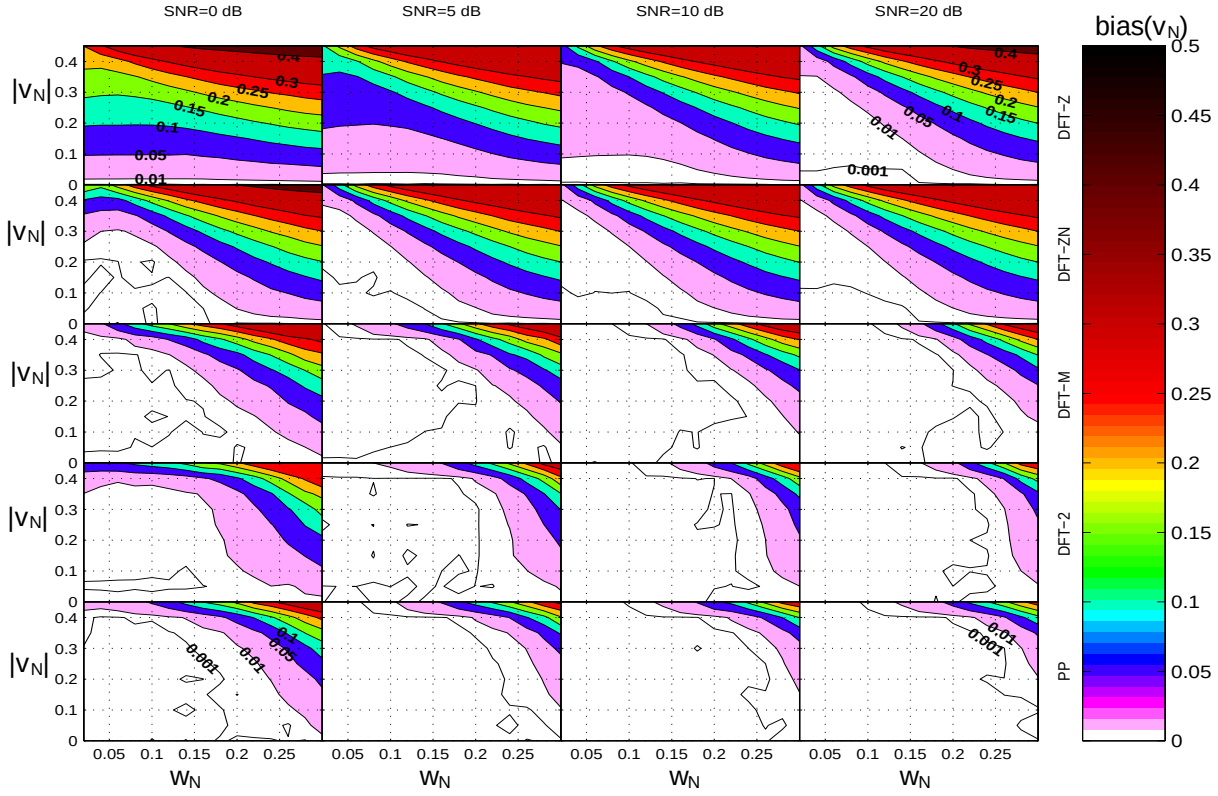

Figure 1: Bias on normalized mean velocity estimates for 5 SME algorithms. In the simulations M=64.

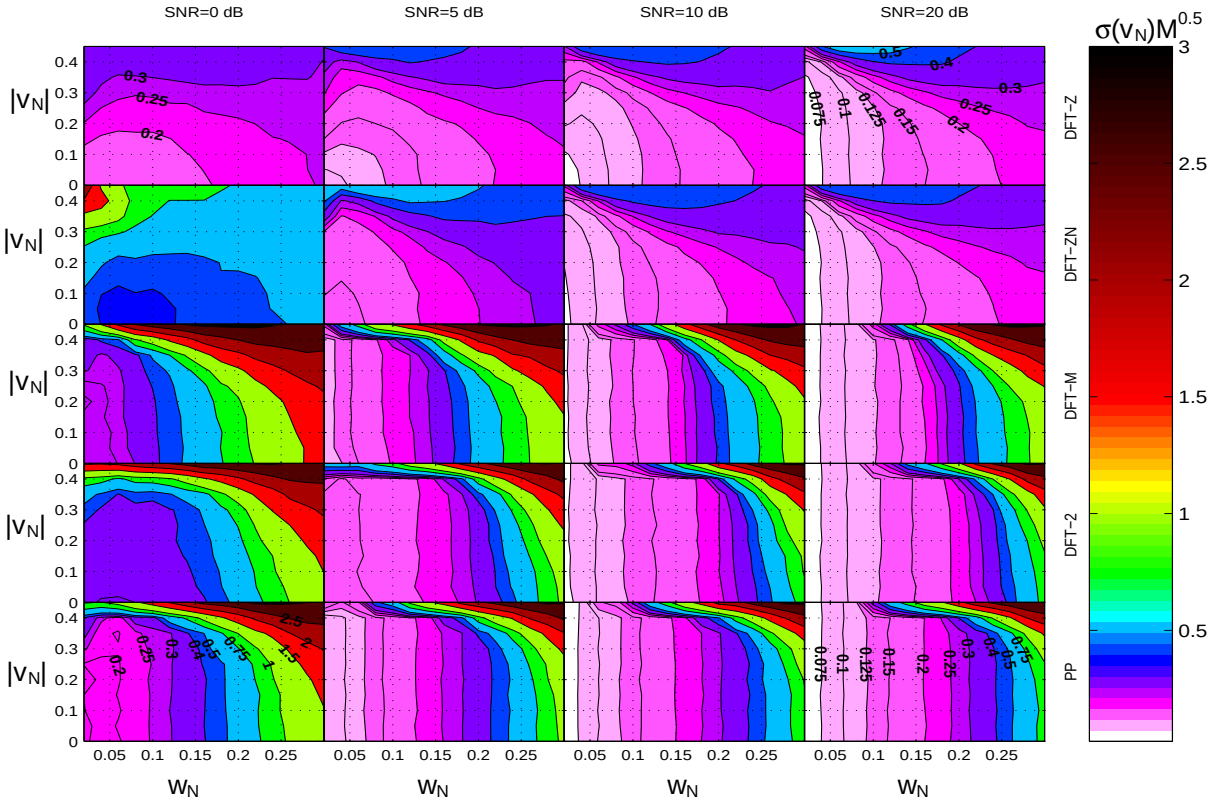

Figure 2: Normalized standard deviation of normalized mean velocity estimates for 5 SME algorithms. The standard deviation is scaled by $M^{0.5}$: such quantity is invariant on M for DFT-Z, DFT-ZN and PP.

to detect if the estimate converged to an aliased replica $v_c \pm 2v_m$, or b) if

$$\sum_{m=m_i'-M/4}^{m_i'+M/4}\left[\tilde{P}_{\mathrm{mod}_M(m)} - \hat{N}_{\mathrm{mod}_M(m)}\right] < \frac{1}{2}\sum_{m=-M/2}^{+M/2}\left[\tilde{P}_m - \hat{N}_m\right]$$

to detect if the estimate converged to $v_c \pm v_m$ in the low power density region of the spectrum.

Estimates of the mean velocity of Gaussian spectra simulated as in Tanelli et al. (2002b) were calculated through these four algorithms and through PP (contiguous pairs). The bias and standard deviation of these estimates are shown in Figs. (1) and (2), respectively. While the estimates of DFT-Z and DFT-ZN are heavily biased by the aliased portions of the spectrum, those obtained through DFT-M, DFT-2 or PP are unbiased for a wide range of w_N and v_N. Among these three, PP shows the smallest standard deviation for low SNR' s and small w_N, DFT-2 shows the smallest standard deviation for high SNR' s and $w_N \geq 0.1$, and DFT-M shows performances between those of PP and DFT-2.

Note that SME performances degrade rapidly when v_N exceeds a threshold that depends on both w_N and the specific SME algorithms used. It was found that such threshold can be approximated by $0.5 - A_R w_N$ where A_R is equal to 1 for DFT-2 and to 1.65 for DFT-M. One can consider as the 'nominal' performances of the algorithm those calculated for $|v_N|$ lower than this threshold.

3. RADAR DESIGN AND DOPPLER SPECTRUM PARAMETERS

In this Section the four parameters of the Doppler spectrum that affect the performance of mean velocity estimators are discussed.

3.1 Normalized Doppler width

For NDPR, the total variance w^2 of the spectrum is calculated as the sum of the variances determined by four different causes of spread (Amayenc et al, 1993):

$$w^2 = w_D^2 + w_T^2 + w_K^2 + w_S^2 \qquad (2)$$

– w_D is due to the spread of terminal fall velocities of hydrometeors of different size. In general, it is determined by the drop-size distribution (DSD) and by the choice of radar operating wavelength. However, it was found that its value is typically $w_D \cong 1$ m/s. The Doppler spectrum associated with the terminal fall velocities is often approximated with a Gaussian, although it is actually slightly skewed, and its mean velocity is typically in the 1 to 7 m/s range.

– w_T is the broadening due to air turbulence. Values for w_T of 1 and 4 m/s are associated with standard and extreme turbulence, respectively. Such broadening is well approximated by a zero-mean Gaussian spectrum.

– w_K is the broadening due to wind shear. Its contribution has been widely studied and a comprehensive discussion of the effect of wind shear for an NDPR with circularly symetric antenna pattern can be found in Kobayashi (2002), whence the following expression is obtained:

$$w_K^2 = \frac{\theta_3^2 h_S^2}{4a}\left(w_{Kzx}^2 + w_{Kzy}^2 + w_{Kh}^2\right) + w_{Kzz}^2 \qquad (3)$$

where , θ_3 is the antenna 3dB width, h_S is the satellite altitude, and

$$\begin{aligned} w_{Kzx}^2 &= \left(u_{x0}/h_S + K_{zx}\right)^2 \\ w_{Kzy}^2 &= \left(u_{y0}/h_S + K_{zy}\right)^2 \\ w_{Kh}^2 &= \frac{\theta_3^2}{4a}\left(K_{xy} + K_{yx}\right)^2 \\ w_{Kzz}^2 &= \left(\frac{0.35 K_{zz} c \tau_{pulse}}{2}\right)^2 \end{aligned} \qquad (4)$$

where $u_i = u_{i0} + jK_{ij}$ with $i=x,y,z$ indicates the direction of the wind component and $j=x,y,z$ indicates the gradient component direction, c is the speed of light and τ_{pulse} is the radar pulse duration. The parameter a depends on approximation used for the antenna pattern (*e.g.*, a =2.6 for the aperture type approximation used in Kobayashi et al. (2002), while a = 4ln(2) ≅ 2.77 for a Gaussian approximation as in Amayenc et al. (1993)). Note that (4) includes also the broadening effect of the average wind components across the beam (*i.e.*, u_{x0} and u_{y0}), this is due to the fact that the associated radial velocity varies with the angle respect to the radar pointing direction. In general, it is found that K ranges between 0.001 s^{-1} to 0.01 s^{-1}.

– w_S is the broadening due to the platform motion. Its effect can be immediately understood through the formalism used for calculating the wind shear by noting that the apparent average wind velocity should be used in (3) (i.e., u_{x0} should be replaced by u_{x0} - v_S, where v_S is the satellite velocity) and therefore:

$$w_S^2 = \frac{\theta_3^2}{4a} v_S^2 \qquad (5)$$

In general, all these causes of spread must be accounted for. However, the following considerations help to simplify the problem:

- Given a v_S of 7 km/s or higher, typical for a Low Earth Orbiting (LEO) satellite, the term w_S prevails over w_{Kzx} and w_{Kzy} and, in particular, for low to medium wind shear (*i.e.*,K<0.005 s^{-1}) the latter two are negligible with respect to w_S for any choice of θ_3.
- Assuming that the wind shear has equal sharing among the orthogonal components, the contribution of w_{Kh} is negligible with respect to w_{Kzx} and w_{Kzy} for small θ_3. Furthermore, w_{Kh} is always negligible with respect to w_S.
- Speceborne atmospheric radars are typically required to have a range resolution of 500 m at least. Therefore the contribution of W_{Kzz} is not negligible with respect to w_{Kzx} and w_{Kzy} only for very small antenna footprints (i.e., for IFOV $\cong \theta_3 h_S$.comparable to 0.35 c τ_{pulse} $a^{0.5} \cong$ 500m.

In general, we have that the Doppler width is determined mainly by the w_S term for $\theta_3^2 >> (w_T\ 2\ a^{0.5}\ /v_S)^2$. That is, for $\theta_3 > 0.15°$ one has that $w \cong w_S$ independently of the amount of turbulence, wind shear and spread of terminal velocities. For smaller beamwidths, instead, the contribution of the three terms depending on the characteristics of the rainfall field cannot be neglected, and, in general, a varying w will be observed by NDPR.

Furthermore we can consider the approximation $\theta_3 \cong \gamma \lambda / D$, where D is the antenna diameter and γ is typically ~1.25. It follows that, given a choice of antenna size, the contributions of w_S and w_K to the normalized spectral width w_N do not depend significantly on λ. On the other hand the contribution of w_D and w_T (which do not depend on θ_3), tend to create broader normalized spectra for smaller λ.

Independently of the aformentioned issues in the choice of antenna size and operating wavelength, a simple criterion to obtain small w_N would be to adopt a high PRF. However, the PRF upper bound is determined by the thickness of the atmosphere layer to be monitored. For precipitation measurements at a scanning angle β we have:

$$\frac{1}{PRF} = T_s > \frac{2H}{c}\frac{1}{\cos(\beta)} \qquad (6)$$

where H is the extent of range interval with non-zero backscatter, in general it can be assumed to be 20 km or less for spaceborne radar measuring precipitation (which accounts also for the presence of the mirror image return). Therefore, PRF up to 8000Hz could be assumed for for scanning strategies with small β. However lower PRF must often be adopted because of the practical problems arising from the long and non-constant slant range of a spaceborne down-looking radar and/or from the choice of using long radar pulses to apply pulse-compression techniques.

Indeed the condition (6) poses a serious obstacle for obtaining low w_N. In fact, while an antenna of 10m could provide spectra with w_N similar to that of airborne radars, obvious economical and technological requirements lead to the choice of smaller antennas, whenever possible. On the other hand, a 2 m antenna such as that of the TRMM Precipitation Radar (PR) or the one planned for the dual frequency precipitation radar of the GPM mission, even if PRF = 8000 kHz is considered, would generate spectra with w_N > 0.3, unsuitable for accurate estimates of any spectral moment. Therefore, antenna diameters between 3 and 6 meters are therefore considered as the region where to look for the optimal trade-off, for the purpose of radar system and mission design. The corresponding range of w_N is between 0.1 and 0.3.

One efficient way to overcome the constraint imposed by (5) is to adopt a pulse polarization diversity strategy as described by Kobayashi (2002). However, this choice increases the technological requirements and is subject to some limitations in its use, among them we mention the fact that DFT processing could not be applied, hence narrowing the choice of SME to the PP category.

***D** [m]*	***2***	***3***	***4***	***5***	***6***	***10***
PRF						
5000	0.50	0.34	0.25	0.20	0.17	0.10
6000	0.42	0.28	0.21	0.17	0.14	0.09
7000	0.36	0.24	0.18	0.14	0.12	0.07
8000	0.32	0.21	0.16	0.13	0.11	0.06

Table (1): Normalized spectral widths w_N as function of (*PRF* and antenna diameter D) for v_s = 7000 m s^{-1} and $w_T = w_D = w_K = 0$.

3.2 Signal to Noise Ratio

The power received at the receiver of a radar can be calculated through the well-known Probert-Jones equation. The radar system parameters that affect its value are the peak power and pulse duration. They have little impact on the issues

pertaining vertical velocity estimation other than the obvious effect on SNR. It can only be mentioned for completeness that a longer τ_{pulse} , while increasing the SNR, also extends the range interval affected by surface clutter and increases the usually negligible term w_{Kzz} in (4).

Spaceborne precipitation radars currently operating or under development guarantee a minimum detectable reflectivity of 17dBZ or less. This means that SNR > 0dB are generally expected when observing rainfall.

In the analysis of the performances of SME algorithms, the noise spectrum has been assumed white to model the radar system thermal noise.

3.3 Normalized mean Doppler velocity

As shown in Section 2, the mean Doppler velocity of the spectrum, which is the object of the estimator, in turn affects the performances of a SME. The reason being that the impact of aliasing becomes drammatically evident when v_N approaches the Nyquist limit of 0.5. This consideration should be taken into account when calculating the maximum vertical velocity that can be calculated with the nominal accuracy of the SME algorithm (see final notes of Section 2).

In practice, average rainfall vertical velocities are generally smaller than v_{Rmax} = 20 m/s in modulus (larger values can occur only for particularly strong up- and down-drafts which usually have very small extension with respect to the radar IFOV). Therefore, one should impose that $(0.5\text{-}A_R\, w_N)\, PRF\, \lambda / 2 > v_{Rmax}$ m/s. When $\theta_3 > 0.15°$ this condition can be reduced to

$$\frac{PRF}{4} - \frac{v_{R\max}}{\lambda} > \frac{A_R v_S}{2\sqrt{a}} \frac{\gamma}{D} \qquad (7)$$

As it will be discussed in Section 5, the impact of velocity offsets caused by errors in the radar pointing angle should be included in v_{Rmax} for robust system design.

3.4 Number of samples

In order to reduce uncertainty on the power spectrum, a sufficiently large number of pulses must be integrated. In Doppler processing, large M also improves the Doppler resolution $v_\Delta = (\lambda/2)/(MT_S)$. A general limitation to the maximum M is imposed by setting the required horizontal spatial resolution, in fact the resolution in the along-track direction is $FOV_x = IFOV + v_S M/PRF$.

If the observed rain process is not stationary during the observation time $T_I = M/PRF$, the Doppler spectrum is distorted due to assemble of the shifting of Doppler velocities of individual rain particles. A reasonably optimal T_I can be found by imposing that the Doppler velocity resolution $v_\Delta = PRF\, \lambda / (2M)$ be equal to the Doppler velocity shift v' during T_I (i.e., $v'=v^2_S T_I/h_S$):

$$T_I = \frac{1}{v_s}\sqrt{\frac{\lambda \cdot h_s}{2}} \qquad (8)$$

If Condition (8) is not satisfied, and a rainfall field inhomogeneous within the field of view is observed, a distortion is introduced in the Power spectrum. As a consequence the performances of SME algorithms will be degraded. Furthermore, this distortion will affect also the performances of more advanced spectral analysis techniques such as the one introduced in the next Section.

4. NUBF-INDUCED BIAS

As recently demonstrated by Tanelli et al. (2002), inhomogeneities in the rain field within the radar volume of resolution cause a shape distortion of the Doppler spectrum and an offset between the mean Doppler velocity and the actual mean vertical velocity of the hydrometeors. Such offset was found to be proportional to the reflectivity gradient in the along-track direction and it can reach values of several m/s. As a consequence a bias equal to the offset affects velocity estimates obtained by means of any SME algorithm when NUBF occurs.

In order to remove such bias, the Combined Frequency Time (CFT) technique has been developed (Tanelli et al. 2001) and it is briefly recalled here. CFT aims at removing the NUBF-induced bias from the estimates of rainfall average vertical velocity by estimating the first moment of the tracks of the rainfall distributed targets projected in the along-track satellite position / Doppler velocity $(x\text{-}v)$ plane. Figure 3 shows a sequence of periodograms measured by a Doppler radar for a fixed range cell. Each periodogram is calculated from the DFT of $M = 64$ complex voltage samples. Therefore one periodogram is obtained in the time T_I which corresponds to an along-track displacement of the satellite $\Delta_x = v_S M/PRF$. The example in Fig. 3 is obtained from a typical NUBF situation where the power spectrum deviates substantially from a Gaussian shape. On the other hand, one can analyze the spectral density lines generated by a specific target at different times (i.e., the 'target tracks' along lines with slope $q_{xv} = v_s/h_s$ in the $x\text{-}v$ plane). It has been demonstrated that, for NDPR,

the target tracks can be well approximated by a Gaussian (from the shape of the antenna pattern), regardless of NUBF. The first moment estimated through a DFT based SME of each target track provides accurate information on both the target position when the target is in the antenna maximum gain direction, and the true vertical velocity of the target. The last step of the CFT technique consists in generating a uniformly spaced horizontal profile of vertical velocity through weighted moving average of the of target velocities obtained for each target track. The moving average 'along-track window' is Gaussian shaped with width Δx.

Results as the one shown in Fig. 4 demonstrate that CFT is able to correct the bias introduced by NUBF.

5 POINTING-INDUCED BIAS

The pointing-induced offset in Doppler velocity is $v_P = \boldsymbol{i_V} \bullet \boldsymbol{i_X} v_S$ where $\boldsymbol{i_x}$ is the along-track direction and $\boldsymbol{i_v}$ is the radar pointing direction. For a nadir-pointing or a cross-track scanning atmospheric radar with no pointing error in the forward-aft direction, this term disappears (*i.e.*, $\boldsymbol{i_V} \bullet \boldsymbol{i_X} = 0$). In actuality, however, several factors can cause error in radar pointing in the forward-aft direction (*e.g.*, attitude determination errors, thermal distortions of the antenna structure, vibrations due to moving parts, slew, thermal flutter or thermal snaps). For v_S = 7 km/s one can note that a misponting error of only 0.1 deg. causes an offset v_P up to 12 m/s. In order to guarantee $|v_P| < 1$ m/s, the rms in the knowledge of the pointing direction should be of 4 arcsecs or less. Such requirement for a LEO satellite poses a technological challenge even for the most sophisticated Attitude Determination Systems.

Recently, Im et al. (2002) proposed to apply the CFT technique to the sea surface echo in order to estimate v_P and therefore remove the pointing-induced bias from mean velocity estimates. The first promising results show that CFT is capable of removing pointing-induced biases introduced from several sources of pointing error.

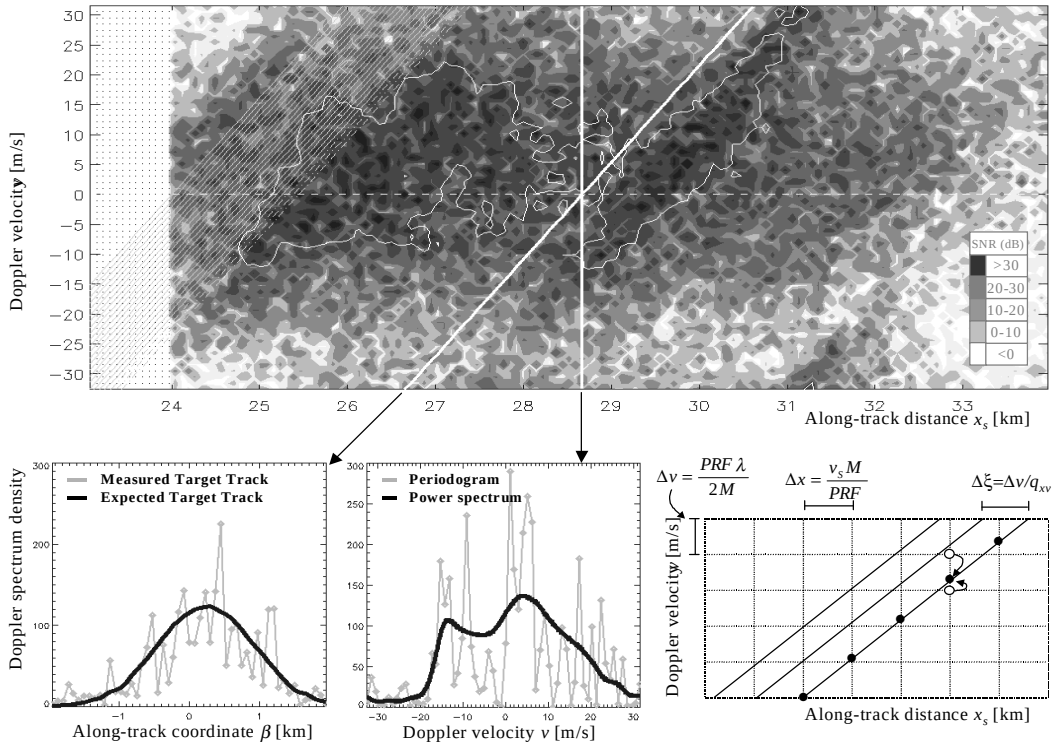

Fig. 3 Application of CFT to sequences of measured Doppler spectra: a) example of sequence of Doppler spectra, white diagonal lines indicate the target tracks, b) target track, c) periodogram, d) interpolation of power spectral samples to obtain measured target tracks.

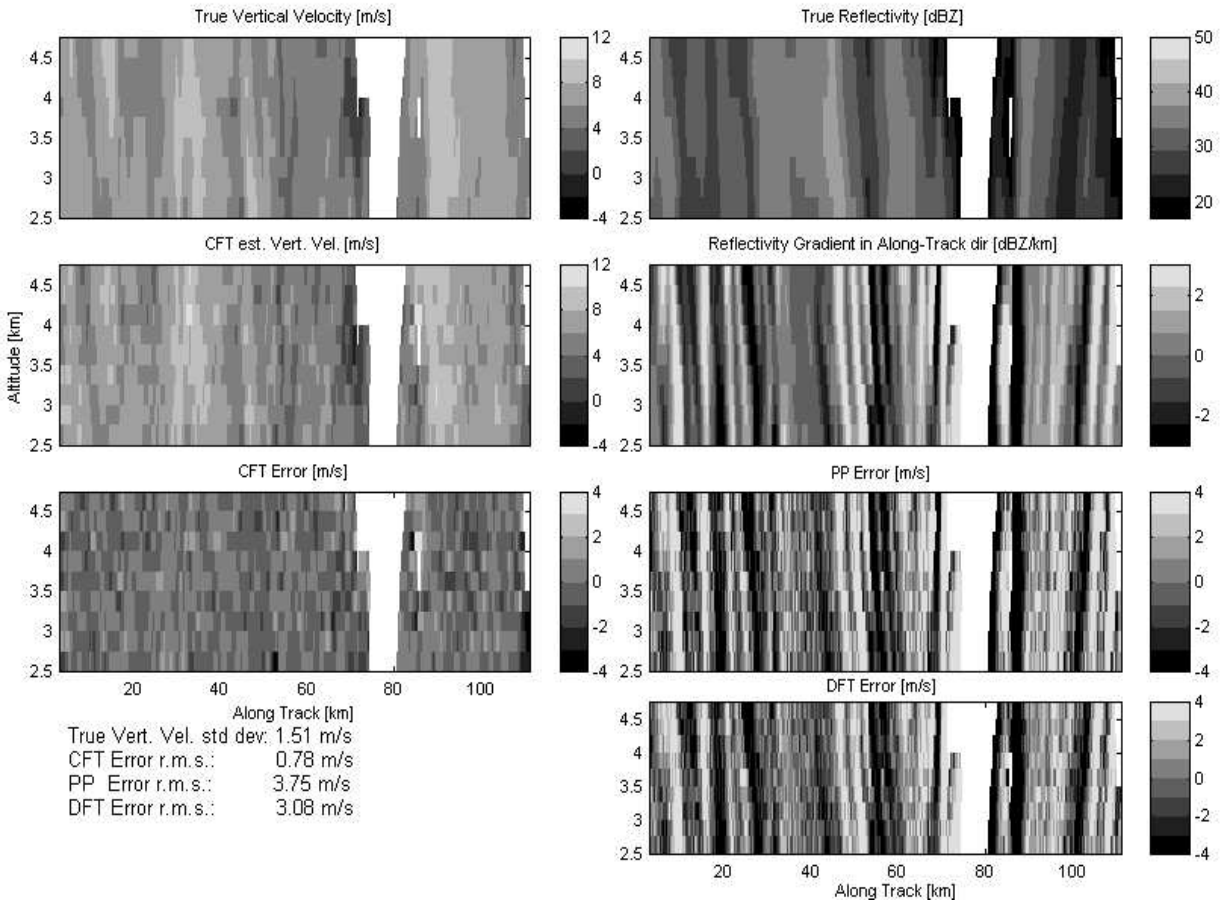

Fig. 4 Vertical section of hurricane ' Bonnie' . ' True' Values are measured by ARMAR at high resoluti The reflectivity gradient is shown sign reversed for better comparison with PP and DFT error plots. rms of the three error plots are shown in the bottom left corner together with the true vertical velocity standard deviation. It is possible to recognize several ' true' vertical velocity features in the CFT reconstruction (which were undetectable in DFT and PP reconstructions).

6. ERRORS INDUCED BY SURFACE CLUTTER

As demonstrated by Durden et al. (2001), the contribution of surface clutter from the sidelobes is typically below the thermal noise level for a nadir-looking radar. Furthermore, since the surface clutter received through the sidelobes is generated by annuli of the sea surface centered at nadir, this contribution can be well approximated with a white spectrum. Therefore, the effect of this contributions can be assimilated to that of white noise discussed previously.

On the other hand, the spectrum of range gates immediately above the surface are heavily contaminated by surface clutter because of the finite receiver bandwidth. Incidentally, as mentioned in the previous section, the Doppler spectrum of the radar cell intersecting the surface is useful to estimate the pointing-induced bias. Such correction is possible by relying on the fact that the sea spectrum is roughly Gaussian and the surface average vertical velocity is zero (Im et. al. 2002). This fact allows also to envisage a spectral analysis technique capable of removing the clutter component of the spectrum from the radar cells affected by mild surface clutter. The development of such technique is of paramount importance to extend (towards the surface) the region of reliable rain echo, especially if the use of pulse compression and/or large β is required.

7. RESULTS AND CONCLUSIONS

The findings and the results described in the previous sections provide the criteria to define several radar system configurations capable of measuring the average rainfall vertical velocity with the 1 m/s accuracy required by most science applications.

One such configuration is described in Table 2.

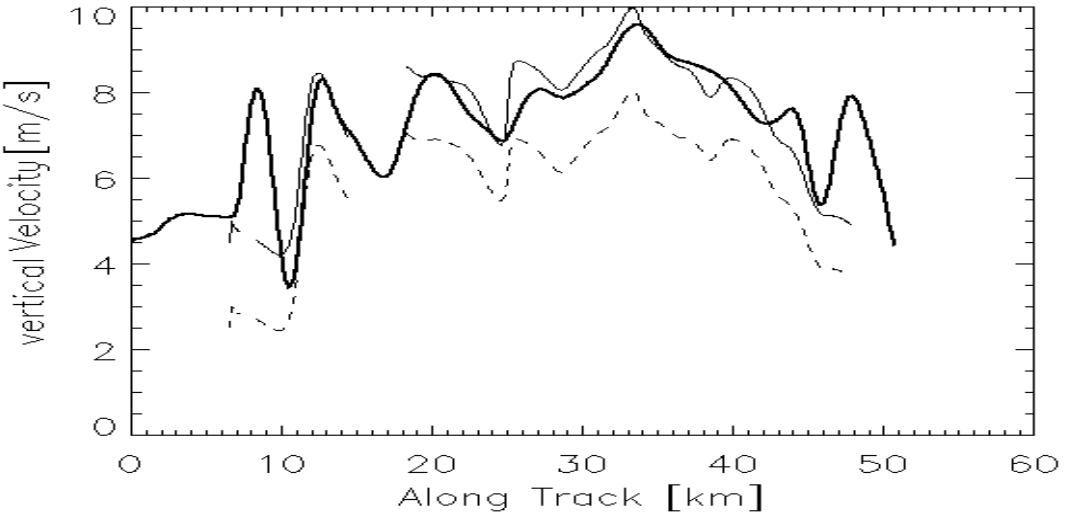

Fig 5. Along track profiles of rainfall vertical velocity: true (v_R , thick solid curve), estimated through CFT with no correction for the pointing angle ($v_{R(CFT)}$, dashed curve), and estimated through CFT with correction for the pointing angle as estimated through CFT processing of the sea surface echo ($v_{R(CFT)} - v_{P(CFT)}$ thin solid curve). The following statistics were calculated: $<v_R - v_{R(CFT)}>$ = 1.68 m/s, $<v_R - v_{R(CFT)} - v_{P(CFT)}>$ = 0.03 m/s, $\sigma(v_R - v_{R(CFT)})$ = 0.83 m/s, $\sigma(v_R - v_{R(CFT)} - v_{P(CFT)})$ = 0.8 m/s.

Satellite speed	v_s	7 km/s
Satellite altitude	h_s	432 km
Pulse repetition frequency	*PRF*	6000 Hz
Operating frequency	f_c	13.6 GHz
Operating wavelength	λ	2.2 cm
Nyquist Doppler velocity	v_m	λ *PRF/4*= 33 m/s
Doppler shift rate	q_{xv}	v_s/h_s= 16.2 m/s km^{-1}
Antenna diameter	*D*	5 m
3dB antenna beamwidth	θ_3	0.3°
"Null-to-null" beamwidth	θ_0	0.75°
Number of pulses	*M*	64
Minimum detectable rain reflectivity	*N*	17 dBZ

Table 2: NDPR configuration I parameters

Simulations were carried out using this set of parameters in a 3D Doppler radar simulator where several sequences of periodograms are simulated from two kind of high-resolution 3-D rainfall data sets: set A, acquired by the NASA/JPL Airborne Rain Mapping Radar (ARMAR, Durden et al. 1994) and set B generated by a Cloud Resolving Model. In this simulation model (Tanelli et al., 2002), each NDPR resolution volume (2.2-km horizontal and 240-m vertical resolution) is divided into several sub-volumes of sizes comparable to those of the ARMAR data (200-m horizontal and 80-m vertical resolution) to account for the presence of NUBF. The natural spectrum of each sub-volume is first computed by taking into account the spread of terminal velocities of different rain particles and the additional broadening due to turbulence and wind shear. The spectrum is then shifted by the radial component of the satellite velocity calculated at the center of the sub-volume, and by the average vertical wind speed derived from ARMAR Doppler measurements. These natural power spectra from all sub-volumes are summed to generate the NDPR power spectrum. The corresponding periodogram is then derived as in Zrnic (1978). Statistical variability of the rainfall signal, receiver' s noise and surface clutter are included in the simulations. The spacecraft attitude errors and antenna misalignements were simulated by a stochastic process with cutoff frequency at 0.25 Hz.

Results of simulations such as that shown in Fig. 4 confirmed that this radar configuration is capable of providing the required level of accuracy. Also, the use of CFT is necessary when NUBF occurs. Furthermore, its application to surface Doppler spectra is useful to correct for the NUBF-induced bias as shown in Fig. 5.

ACKNOWLEDGMENT

The research described in this paper was performed at the Jet Propulsion Laboratory, California Institute of Technology, under contract with the National Aeronautics and Space

Administration, and by the University of Firenze through a program funded by ASI (Italian Space Agency).

REFERENCES

Amayenc P., J.Testud and M.Marzoug, 1993: Proposal for a spaceborne dual-beam rain Radar with Doppler capability, *J. Atm. Oce. Tech.*, **10**, pp.262-276.

Doviak R.J. and D.S. Zrnic, 1993: *Doppler radar and weather observations*, Academic Press.

Durden S.L., E.Im, F.K.Li, W. Ricketts, A.Tanner and W.Wilson, 1994: ARMAR: An Airborne Rain-Mapping Radar. *J. Atmos. Oceanic Technol.,* **11**, 727-737.

--, --, --, R.Girard and K.S.Pak, 2001: Surface clutter due to antenna sidelobes for spaceborne atmospheric radar. *IEEE Trans. on Geosc. and Rem. Sens.,* **39**, n.9, pp. 1916-1921

Hildebrand P.H. and R.K.Moore, 1990: Meteorological Radar Observations from Mobile Platforms, in *Radar in Meteorology,* D.Atlas Ed. Boston, MA: American Meteor. Soc., ch. 22a, pp-286-314

Im E., S. Tanelli, R. Mascelloni and L. Facheris 2002: Spaceborne rainfall Doppler radar measurements: correction of errors induced by pointing uncertainties, *to appear on Proc. of Third International Asia-Pacific Symposium on Remote Sensing of the Atmosphere, Environment and Space* (SPIE Vol 4894), Hangzhou (RPC), Oct. 23-27 2002.

Kobayashi S, 2002: A Unified formalism of incoherent, quasi-coherent, and coherent correlation signals on Pulse-Pair Doppler operation for a cloud-profiling radar: aiming for a space mission. *J. Atm. Oce. Tech.*, **19**, pp.443-456.

--, H. Kumagai, H. Kuroiwa, 2002 : A proposal of pulse-pair Doppler operation on a spaceborne cloud-profiling radar in the W band. *J. Atm. Oce. Tech.*, **19**, pp.1294-1306.

Sirmans D. and B. Bumgarner, 1975: Numerical comparison of five mean frequency estimators. *J. Appl. Meteor.*, **14**, 991-1003.

Tanelli S., E. Im, S. L. Durden, L. Facheris and D. Giuli, 2002: The effects of nonuniform beam filling on vertical rainfall velocity measurements with a spaceborne Doppler radar, *J. Atmos. Oceanic Technol.,* **19**, 1019-1034.

--, --, Luca Facheris and Eric A. Smith, 2002 DFT-based spectral moment estimators for spaceborne Doppler precipitation radar, *to appear on Proc. of Third International Asia-Pacific Symposium on Remote Sensing of the Atmosphere*, Environment *and Space* (SPIE Vol. 4894), Hangzhou (RPC), Oct. 23-27 2002.

--, --, -- and S.L.Durden, 2001: Signal processing technique for removal of NUBF induced error in spaceborne Doppler precipitation radar measurements, *Proc. of SPIE International Symposium on Remote Sensing – Remote Sensing of Clouds and the Atmosphere VI*, Toulouse (F), Sept. 17 – 21, (SPIE vol 4539), p. 221-232.

Zrnic D.S. 1978: Simulation of weatherlike Doppler Spectra and Signals, *J. App. Meteor.*, **14**, pp. 619-620

--, 1979: Estimation of spectral moments for weather echoes. *IEEE Trans. On Geosc. Electr.*, **4**, 113-128.